machines

MDPI

Article

Analysis of the Electrical Impedance of Graphite and Silver Graphite Carbon Brushes for Use in the Impedance Measurement of Sensory Utilizable Machine Elements

Maximilian Hausmann [1,*], Tobias Schirra [2] and Eckhard Kirchner [1]

[1] Department of Mechanical Engineering, Institute for Product Development and Machine Elements, Technical University of Darmstadt, 64287 Darmstadt, Germany; kirchner@pmd.tu-darmstadt.de
[2] HCP Sense GmbH, 64287 Darmstadt, Germany; schirra@hcp-sense.com
* Correspondence: maximilian.hausmann@tu-darmstadt.de; Tel.: +49-6151-16-21191

Abstract: The ongoing digitalization of processes and products in mechanical engineering is accompanied by an increasing demand for data. In order to provide this data, technical systems are being extended with sensory functions. To supply those sensory functions on rotating elements—such as shafts—with electrical energy, and to be able to transmit signals out of the system, sliding contacts can be used as a cost-effective and established solution. However, if electrical properties of machine elements are utilized for sensing purposes, such as condition monitoring of rolling element bearings by means of impedance measurement, sliding contacts are directly in the measurement path and can thus influence the measured impedance. The aim of this paper is to analyze the impedance of graphite and silver graphite carbon brushes under different rotational speeds, in different positions, and with different carrier frequencies. The material of the carbon brushes as well as the position have significant effects on the impedance behavior. Furthermore, carbon brushes show a significant running-in behavior. The results are discussed, and indications for use in impedance measurements are given. Silver graphite carbon brushes in axial positioning are particularly suitable for impedance measurements of sensory utilizable machine elements. Sufficient running-in time must be considered.

Keywords: digitalization; sensor integration; sensing machine element; sensory utilizable rolling element bearing; sliding contact; impedance analysis

Citation: Hausmann, M.; Schirra, T.; Kirchner, E. Analysis of the Electrical Impedance of Graphite and Silver Graphite Carbon Brushes for Use in the Impedance Measurement of Sensory Utilizable Machine Elements. *Machines* **2023**, *11*, 1009. https://doi.org/10.3390/machines11111009

Academic Editor: Vincenzo Niola

Received: 4 October 2023
Revised: 27 October 2023
Accepted: 31 October 2023
Published: 3 November 2023

1. Introduction

The ongoing digitalization of processes and products in mechanical engineering serves to implement control tasks, condition monitoring and predictive maintenance, to increase productivity, and establish new business models [1,2]. A basis for this is the availability of usable data of sufficient quality and quantity. A wide variety of sensors can be used for data acquisition. However, the requirements that must be met by the sensor solutions are also continuously increasing [3]. For example, additional installation space required for sensor and auxiliary elements must be kept to a minimum. The sensor solution should also have as little negative impact as possible on the technical system; e.g., due to component weakening, and should also be as robust as possible in regard to potential disturbance variables. The complexity must also be kept to a manageable level; e.g., by using standardized electrical and mechanical interfaces. In addition to these requirements, there are many more, but a focus on these is sufficient to motivate this contribution.

One technical possibility for implementing highly integrated sensory functions are so-called mechatronic machine elements [4]. Sensing machine elements are derived from mechatronic machine elements [5]. These are conventional and standardized machine elements which are extended by one or more sensory functions with as few modifications as possible. On one hand, the sensor and auxiliary elements can be integrated on or in the machine element. On the other hand, it may also be possible to use the electrical

properties of the machine element in operation directly in a sensory manner—so-called sensory utilizable machine elements (SuME). One example of this innovative approach are sensory utilizable gears that are subject to ongoing research activities; e.g., [6–8]. The impedance of the gear mesh, which is directly dependent on the lubrication condition and the proportion of mixed friction [9,10], is to be used to derive conclusions regarding rotational speed, acting torque, and potentially surface damage. Another example are sensory utilizable rolling element bearings that have been subject to research activities for many years—e.g., [11–15]—and are currently being brought to production maturity in the industry; e.g., [16]. As shown in Figure 1, the electrical capacitance of a rolling element bearing is measured—e.g., by a suitable impedance measurement of Z_{DUT}—and used for sensory purposes on the basis of the relationship between lubrication film thickness and capacitance. Due to their influence on the lubrication film thickness, conclusions can be drawn about acting loads, applied rotational speeds, present temperatures, or even damages in the raceways.

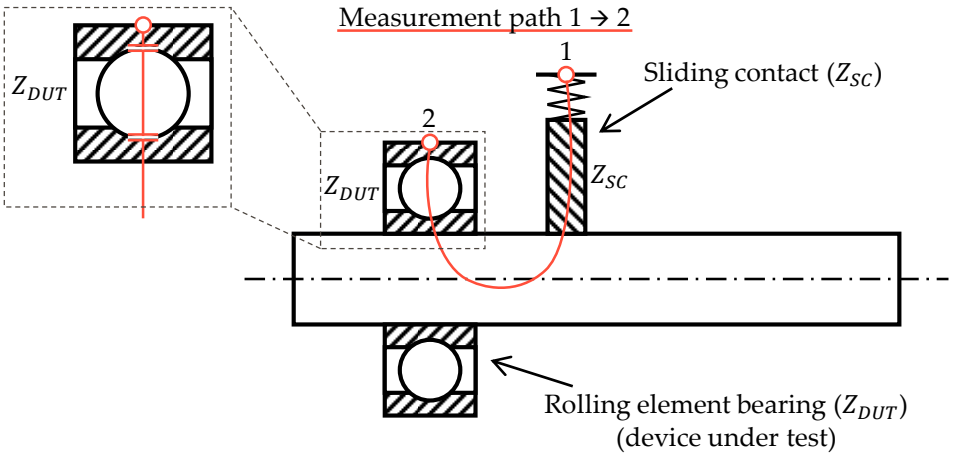

Figure 1. Measurement path from contact point 1 to contact point 2 for the sensory utilization of a rolling element bearing via impedance measurement. The impedance of the sliding contact Z_{SC} is connected in series with the impedance of the rolling element bearing Z_{DUT}.

Since additional elements for energy supply and storage as well as for signal processing and transmission are omitted as far as possible in case of SuME, the actual development of SuME represents only a part of current challenges. If SuME are to be integrated into or onto rotating systems—e.g., on a shaft—as is the case with sensory utilizable gears and rolling element bearings, two main questions arise in addition to the actual development of the sensory function:

- How is the sensory function supplied with energy?
- How is the sensor signal transmitted out of the rotating system to the evaluation unit?

At the moment, sliding contacts are often used for test rigs and applications of SuME on rotating systems; e.g., [6–8,12–15]. These are specialized elements, such as carbon or steel brushes, which are pressed onto the rotating element by means of—e.g., a preloaded spring. In this way, uniform and interruption-free electrical contacting can be achieved. As can be seen in Figure 1, this electrical contacting approach represents a part of the measurement path from contact point 1 to contact point 2 of SuME. The measured impedance thus consists of the impedance of the device under test (DUT) Z_{DUT}, and connected in series, the impedance of the sliding contact Z_{SC}.

In order to measure the capacitance of the rolling element bearing in operation, the stationary outer ring and the rotating inner ring must be electrically contacted. Thus, not only is the capacitance of the rolling element bearing measured, but also the electrical properties of the sliding contact, which contacts the rotating shaft near the inner ring. Commonly used compensation approaches to eliminate the cable and contacting impedances from the

measured impedance cannot be applied in these experimental setups without constructive modifications. Such necessary modifications would limit the general usability and the possibility of retrofit solutions for SuME.

Although sliding contacts are described extensively in the literature—e.g., [17,18]—and used in both research and industrial practice, there is still no comprehensive understanding of their influence on impedance measurements in the context of SuME. Despite initial studies of the electrical behavior of sliding contacts in this context [19,20], random sliding contacts are often selected for test setups without having systematically chosen a suitable solution; e.g., [6–8,12–15]. Thus, sliding contacts in applications differ by the material used, the relative contact position to the rotating element, and other parameters. The aim of this contribution is to systematically investigate and qualitatively describe the influences of sliding contacts on impedance measurements in the context of SuME. For this purpose, a suitable experimental setup is designed in which sliding contacts of different materials can be examined at different rotational speeds and in different relative positions to the rotating element. These factors are then varied at two levels each, and the resulting effects on the measurable impedance are evaluated and discussed. The aim is to gain an understanding of the conditions under which sliding contacts can be used in the context of impedance measurements for SuME, how the influence on the measurable impedance may look, and how potential influences can be controlled.

2. Materials and Methods

As already described in the previous section, potential effects of three identified factors on the electrical impedance of sliding contacts are to be systematically investigated. The factors to be considered are the material, the rotational speed of the shaft, and the relative positioning of the sliding contacts to the rotating shaft, as these are variable factors in SuME applications. In a first screening experiment, potential effects on the impedance are to be identified and examined for significance in accordance with design of experiment approaches, and using the analysis of variance method ANOVA [21]. The ANOVA is performed with the help of suitable functions of the 'Statistics and Machine Learning Toolbox' for the software MATLAB R2023a [22]. For this screening purpose, the three factors mentioned are varied according to Table 1 on two levels each. Graphite and silver graphite carbon brushes from Josef Mack GMBH & Co. KG (Grünberg, Germany) are used as materials [23]. These are common materials, which therefore form a suitable basis for initial experiments. The rotational speed of the shaft is varied at levels of 500 rpm and 2000 rpm. The corresponding sliding speeds for the radii used are given in Table 1. This gives an overview of a typical rotational speed range in which there is still minimal risk of the carbon brushes lifting off. Special applications with very high rotational speeds, such as tool spindles, would be associated with significantly higher requirements on the experimental setup, as well as the sliding contacts, and are therefore not considered. The position of the sliding contact can be in axial as well as radial directions. The carrier frequency typically depends on the application. Through preliminary tests at the institute, the value of the carrier frequency for these experiments was set to a constant 100 kHz.

Table 1. List of factors and factor levels for the initial screening experiment.

Factor	Level−	Level+
Material	Graphite [1]	Silver graphite [1]
Rotational speed	500 rpm	2000 rpm
Sliding speed for $r_a = 10.5$ mm	0.55 m/s	2.2 m/s
Sliding speed for $r_r = 15$ mm	0.79 m/s	3.1 m/s
Position	Axial	Radial

[1] Exact material mixture unknown, as it was not specified by manufacturer.

The three factors described above are investigated in a target-oriented two-stage full-factorial experimental design. Due to the feasible effort of a full-factorial design, a

fractional factorial design is not used. Each factor level combination is independently set and measured three times for 2 s each. After setting a factor level, the experimental setup runs for 5 min under the set operating conditions before the measurement is performed. This also applies if the operating conditions should not change. In this case, a waiting time of 5 min between measurements is maintained with the set operating conditions. In order to reduce the probability of systematic errors, the experiments are performed in a randomized order. The randomization was performed with the help of an online random number generator [24]. Due to the high effort of switching between axial and radial contacting, axial and radial tests are performed in separate blocks. However, within these blocks, the previously mentioned randomization takes place. The resulting test sequence used in the screening design is listed in Table 2. The results of this series of experiments are given in Section 3.2.

Table 2. Two-stage full factorial experimental design with blocks for axial and radial contacting and randomization inside both blocks.

Material	Rotational Speed	Position	Repetition	Test Number (Randomized)
Silver graphite	500 rpm	Axial	1	5
Silver graphite	2000 rpm	Axial	1	7
Graphite	500 rpm	Axial	1	10
Graphite	2000 rpm	Axial	1	2
Silver graphite	500 rpm	Axial	2	3
Silver graphite	2000 rpm	Axial	2	8
Graphite	500 rpm	Axial	2	1
Graphite	2000 rpm	Axial	2	9
Silver graphite	500 rpm	Axial	3	6
Silver graphite	2000 rpm	Axial	3	4
Graphite	500 rpm	Axial	3	12
Graphite	2000 rpm	Axial	3	11
Silver graphite	500 rpm	Radial	1	24
Silver graphite	2000 rpm	Radial	1	19
Graphite	500 rpm	Radial	1	14
Graphite	2000 rpm	Radial	1	21
Silver graphite	500 rpm	Radial	2	20
Silver graphite	2000 rpm	Radial	2	22
Graphite	500 rpm	Radial	2	13
Graphite	2000 rpm	Radial	2	23
Silver graphite	500 rpm	Radial	3	18
Silver graphite	2000 rpm	Radial	3	15
Graphite	500 rpm	Radial	3	16
Graphite	2000 rpm	Radial	3	17

Since a specific value of 100 kHz for the carrier frequency is defined for the first experimental series, but in practice this must be selected for a specific application, various carrier frequencies are investigated in the second experimental series. In order to keep the experimental effort manageable, a constant operating point with appropriate impedance values (see Section 3.2) is selected: Silver graphite carbon brush in axial position at 500 rpm. The carrier frequency is swept in a range from 1 kHz to 1 MHz. In addition, the runtime-dependent behavior is to be investigated; therefore, the frequency sweeps are repeated at regular intervals over a total period of 120 min. The results for this series of experiments are given in Section 3.3.

A suitable experimental setup was designed and built for the experimental investigation. With this setup, potential effects of different materials, positions, and rotational speeds on the impedance can be analyzed. Figure 2 shows the complete experimental setup. On the left side, a steel shaft (1) with a diameter of 30 mm is electrically contacted by two carbon brushes. A fixed reference contact point is always located in the rotational axis on the face of the shaft (2), and is not changed during the experiments. A silver graphite

carbon brush is used as a reference. The second contact position can either be slightly offset on the shaft face (3.1, axial contact, $r_a = 10.5$ mm), or on the lateral surface of the shaft (3.2, radial contact, $r_r = 15$ mm). This way, there is always a measurement path over two sliding contacts, with the variable contact position representing a factor as described above. The main shaft (4), which is made of polypropylene, is driven by an electric motor (5) and can be adjusted to various speeds. The shaft is supported by two pillow block bearings (6), and is connected to the steel shaft via a flange connection (7). The plastic design of the main shaft provides electrical insulation between the measurement path over the sliding contacts and the environment, as well as the electric motor. Interference from outside as well as parasitic current paths are thus reduced. The entire experimental setup is set up in a temperature chamber so that the environmental temperature can be regulated to a constant level of 20 °C. Furthermore, the steel shaft is cleaned of lubricants and other contaminants with suitable cleaning equipment before the experiments.

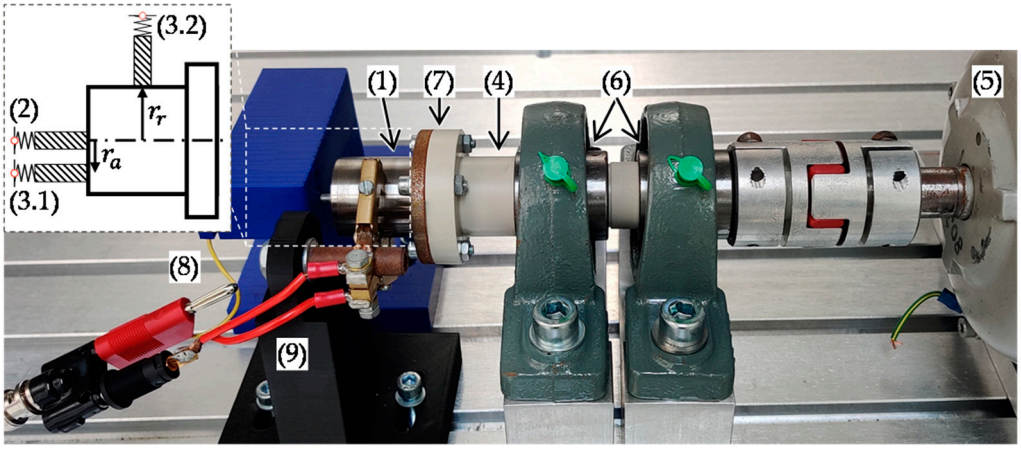

Figure 2. Experimental setup: (1) Steel shaft; (2) Reference contact in axial position (silver graphite); (3.1) Axial contact; (3.2) Radial contact; (4) Insulated main shaft; (5) Electric motor; (6) Pillow block bearings; (7) Flange connection; (8) Connection of reference contact to ground (yellow cable); (9) Connection of axial or radial contact (red cable).

The impedance measurement system consists of an impedance analyzer of type MFIA from Zurich Instruments AG (Zurich, Switzerland) [25]. The MFIA is used in a special measurement setup to measure the impedance of a grounded DUT. In this case, Z_{DUT} is the impedance of the sliding contacts. Details of this measurement setup and the impedance calculation, as well as a detailed electrical circuit, can be obtained from Zurich Instruments AG [26]. This measurement setup is chosen for reasons of comparability, because in many cases one contact side of a sensory utilizable rolling element bearing is directly connected to ground—e.g., via gearbox housing or shafts in industrial applications—where insulations cannot be implemented without extensive design effort. In this experimental setup (see Figure 2), the reference contact on the face of the shaft, and thus the shaft itself, is connected to ground (8). The axial or radial contact to be measured is connected to the measurement device (9).

3. Results

In the following section, the experimental results are presented, described, and interpreted. For this purpose, Section 3.1 first gives an overview of the experimental results and the general impedance behavior of the observed sliding contacts. In Section 3.2, the experimental results of the screening design are examined with respect to potential effects on relevant features of the electrical impedance, and the significance of those potential effects is investigated. Finally, in Section 3.3, the frequency-dependent and the runtime-dependent impedance behavior of sliding contacts is investigated.

3.1. Overview of Experimental Results

Figure 3 shows the measurement results of silver graphite carbon brushes at a constant rotational speed of 500 rpm. Figure 3a shows the results of three test repetitions for an axial contact, and Figure 3b shows the results of three test repetitions for a radial contact. First, it can be observed that there are partly large differences between the three test repetitions of an investigation. It can be deduced that either exactly uniform test conditions are not achieved, or disturbance variables not previously considered are acting in a significant way on the system. Despite this behavior, the measurement results are suitable for further investigations.

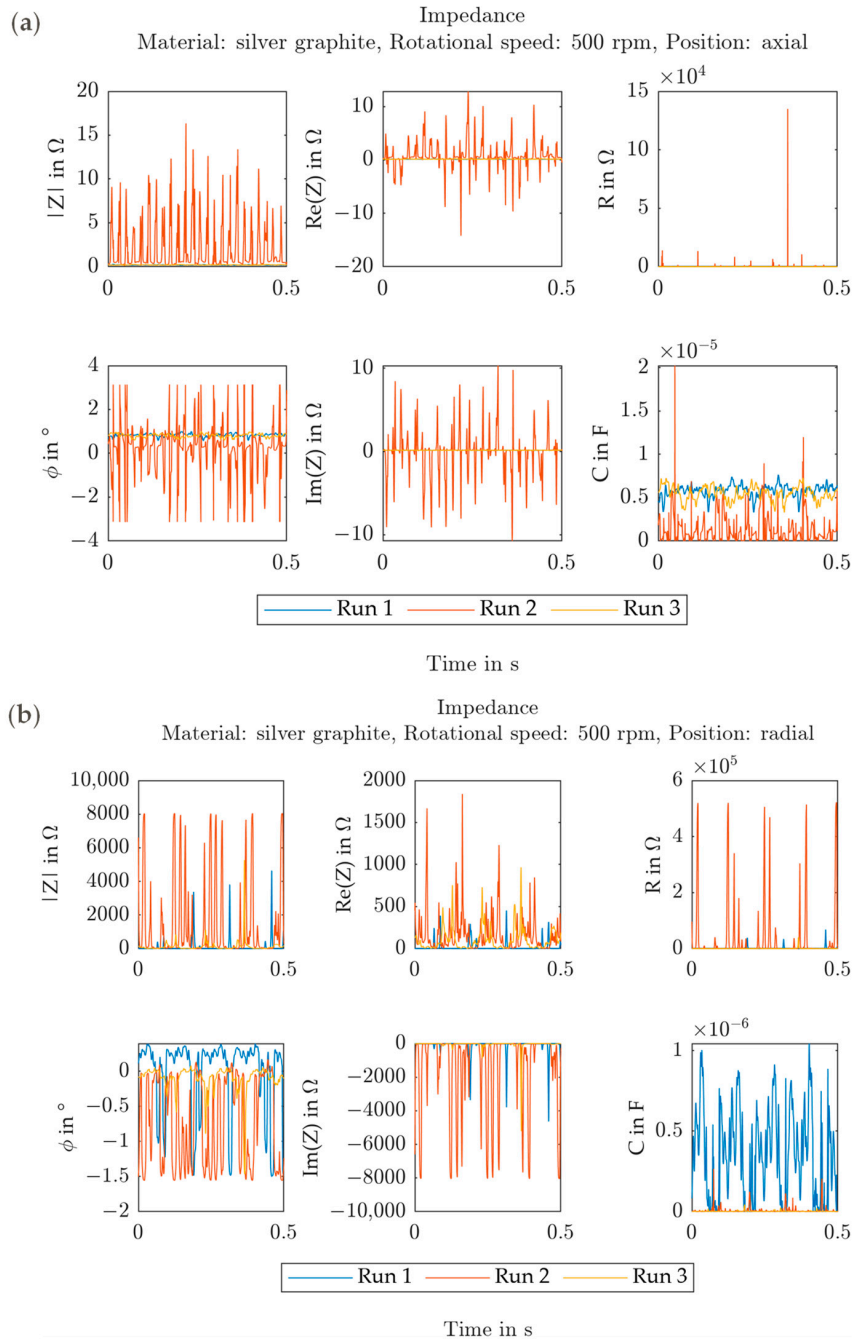

Figure 3. Impedance data over 2 s for silver graphite carbon brushes at a constant rotational speed of 500 rpm and 100 kHz carrier frequency for three individual measurement runs: (**a**) the axial contact shows a smaller but noisier impedance; (**b**) the radial contact shows a larger but less noisy impedance.

For axial contacting, it can be seen in Figure 3a that the measured impedance is very low in terms of absolute value. The phase angle of almost 0° indicates purely resistive behavior. The resistance is very low, with the exception of individual outliers. The real and imaginary parts oscillate around 0 Ω. It can be concluded from this that axial contact using silver graphite carbon brushes exhibits a low and relatively constant impedance. Since a very low resistive impedance is measured, the measurement noise and the measurement uncertainty of the measurement system have a relatively high proportion. This also explains the partially negative real part, which—however—does not play a critical role here.

A significantly higher impedance can be seen for radial contacting in Figure 3b. The phase angle is still almost 0°, and thus still indicates resistive behavior. A significantly higher proportion of very high resistance values, which occur regularly, can be seen. An initial fast Fourier transform (FFT) could not identify any correlation between the rotational speed and peaks of the outliers here. However, it must be pointed out that the impedance analyzer has an integrated low-pass filter activated, and thus high frequencies are reduced. This circumstance became known only after the test executions. The real part shows only positive values, the imaginary part only negative values. Overall, it can be deduced that the impedance exhibits a significantly more transient behavior with radial contacting using silver graphite carbon brushes. This may be due, among other things, to irregularities in the radial contact zone between the shaft surface and the carbon brush, such as scratches and remaining contaminants, as well as dynamic processes such as vibrations of the carbon brush.

3.2. Identification and Evaluation of Significant Effects on the Electrical Impedance

After an initial overview of the electrical behavior of sliding contacts, the significance of potential effects of the factors material, position, and rotational speed on the electrical impedance will be investigated in the following section. An independent ANOVA test is performed for each feature. The detailed results are available in Tables A1–A6 in Appendix A. For the evaluation of the significance of the effects, the resulting *p*-values are used in this section. An independent feature is considered significant if the *p*-value is less than 0.5. The features considered in this work are the absolute value of the impedance—$|Z|$, the phase angle of the impedance—$\varphi(Z)$, the real part of the impedance—$Re(Z)$, the imaginary part of the impedance—$Im(Z)$, the resistance—R, and the capacitance—C. It is important to note that these features are not independent of each other. However, they are used in this work because they can be used to provide different views of electrical impedance.

3.2.1. Effect and Significance of Material

Table 3 contains the *p*-values as results of the ANOVA for factor material on the various features of the electrical impedance. It can be seen that the effects of factor material on the phase and the real part of the impedance—as well as the capacitance—are significant because their *p*-values are lower than 0.05. Figure 4 shows the respective effects graphically.

Table 3. Results of the ANOVA for the factor material related to different features.

Feature	Symbol	*p*-Value	Significance [2]
Absolute value	$\|Z\|$	0.71684	
Phase	$\varphi(Z)$	0.00854	X
Real part	$Re(Z)$	0.03101	X
Imaginary part	$Im(Z)$	0.85401	
Resistance	R	0.79021	
Capacitance	C	~0.00001	X

[2] Significant when *p*-value < 0.05.

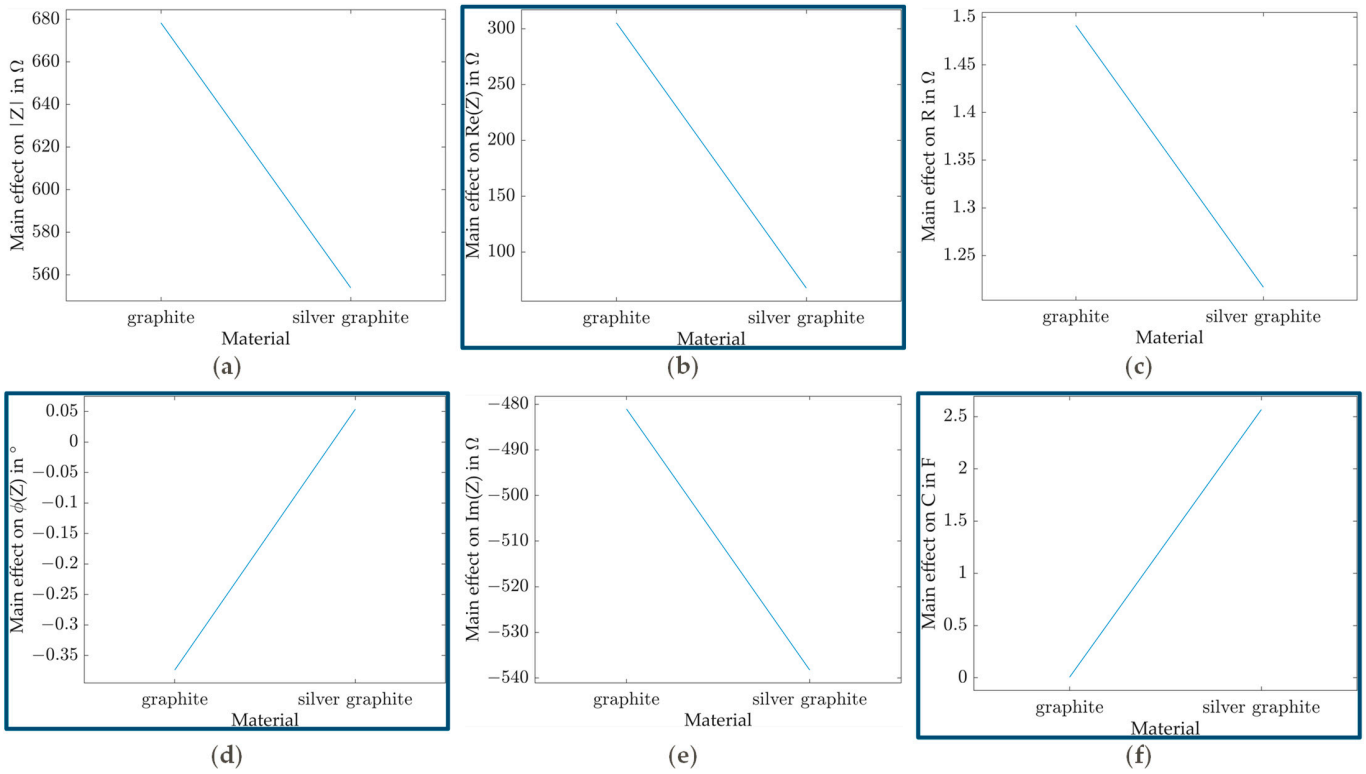

Figure 4. Main effect diagrams of the factor material for different features. Effects significant according to ANOVA (see Table 3) are outlined: (**a**) No significant effect on $|Z|$; (**b**) Significant effect on $Re(Z)$, silver graphite decreases real part; (**c**) No significant effect on R; (**d**) Significant effect on $\varphi(Z)$, silver graphite increases phase to 0°; (**e**) No significant effect on $Im(Z)$; (**f**) Significant effect on C, silver graphite increases capacitance.

In the following, so-called effect diagrams are used for the representation of the effects of factors. The two levels of a factor are plotted on the abscissa. The mean values of a feature are plotted on the ordinate. Here, a mean value of the feature is calculated for all experiments in which the factor under consideration is set to its lower level, and a mean value of the feature is calculated for all experiments in which the factor under consideration is set to its higher level. This results in two points connected by a line. If this line points upwards, it implies a positive effect, and if this line points downwards, it implies a negative effect of the considered factor on the feature. However, the diagram does not yet indicate whether an effect is significant. For this purpose, the ANOVA already presented is used. More information about effects and effect diagrams can be obtained in the literature; e.g., [21].

Figure 4d shows the significant effect of the material on the phase of the impedance. The phase angle for graphite carbon brushes is significantly more negative than the phase angle for silver graphite carbon brushes, which tends towards 0°. It can be inferred that silver graphite carbon brushes exhibit significantly more resistive behavior, although graphite carbon brushes also do not exhibit a strong capacitive behavior. These observations can also be seen in Figure 4b,f, as these characteristics are interdependent. Silver graphite carbon brushes exhibit a significantly higher capacitance, which in turn results in a significantly lower imaginary part of the impedance, and thus a phase angle of 0°. The larger capacitance is potentially due to different material properties as well as the contact area and thickness of a capacitive separation layer. Since the contact area between graphite and silver graphite carbon brushes remains unchanged, the effect can probably be attributed to differently pronounced capacitive layers in the sliding contact, or material properties.

3.2.2. Effect and Significance of Contacting Position

Table 4 contains the *p*-values as results of the ANOVA for factor position on the various features of the electrical impedance. It can be seen that the effects of factor position on the absolute value, the phase, and the imaginary part of the impedance as well as the resistance and the capacitance are significant. Figure 5 shows the respective effects graphically.

Table 4. Results of the ANOVA for the factor position related to different features.

Feature	Symbol	*p*-Value	Significance [3]
Absolute value	$\|Z\|$	0.01630	X
Phase	$\varphi(Z)$	~0.00001	X
Real part	$Re(Z)$	0.52112	
Imaginary part	$Im(Z)$	0.00816	X
Resistance	R	0.01810	X
Capacitance	C	~0.00001	X

[3] Significant when *p*-value < 0.05.

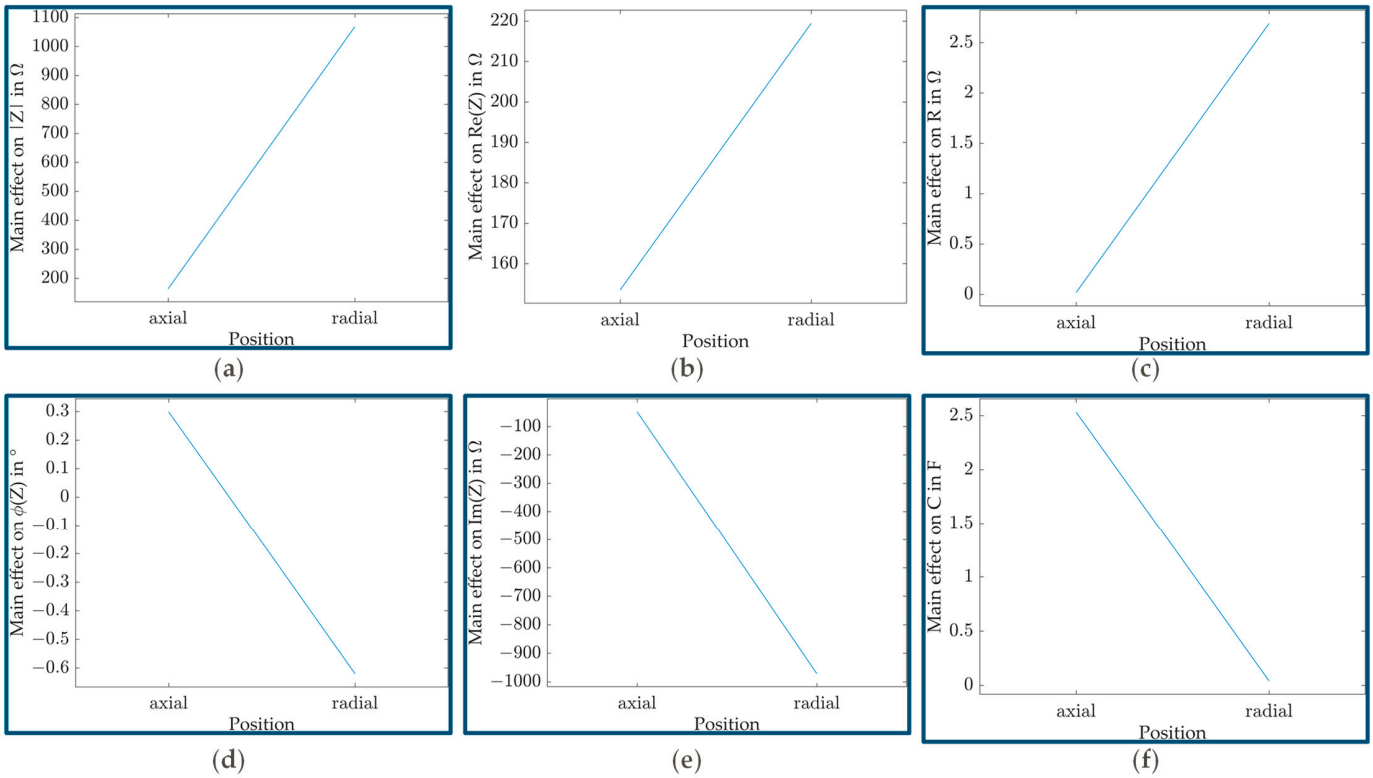

Figure 5. Main effect diagrams of the factor position for different features. Effects significant according to ANOVA (see Table 4) are outlined: (**a**) Significant effect on $|Z|$, radial contact increases absolute value; (**b**) No significant effect on $Re(Z)$; (**c**) Significant effect on R, radial contact increases resistance; (**d**) Significant effect on $\varphi(Z)$, radial contact decreases phase; (**e**) Significant effect on $Im(Z)$, radial contact decreases imaginary part; (**f**) Significant effect on C, radial contact decreases capacitance.

Figure 5a shows that the absolute value of the impedance is significantly greater for radial contacting than for axial contacting. Furthermore, the phase angle of the impedance shown in Figure 5d is also more negative for radial contacting. In principle, however, resistive behavior can be assumed in both cases. Two conclusions can be drawn from these observations together with the dependent effects for resistance (radial contact significantly higher resistance than axial contact, see Figure 5c) and capacitance (radial contact significantly lower capacitance than axial contact, see Figure 5f): First, the axial contact has a uniform and larger contact area at a lower contact speed, which causes the contact

resistance to decrease. Secondly, the larger contact area and the more uniform and smaller contact distance in the axial contact result in greater capacitance when a capacitively acting layer is formed between the contact partners. From this, it can be deduced that the contact resistance increases with radial contact due to a smaller contact area, and at the same time, the capacitance increases due to a smaller area and a larger distance. Both effects are reflected in a greater impedance and a more negative phase angle for the radial contact.

The different contact speed between axial and radial contacting is due to different radii of the contact positions. The axial contact has a smaller distance r_a to the axis of rotation of the shaft in order to be able to act on the face of the shaft. The distance r_r of the radial contact depends on the fixed shaft radius, which at the same time corresponds to the greatest possible distance from the axis of rotation and the highest contact speed. Figure 2 shows this situation with the associated radii. The different contact surfaces between axial and radial contacting are attributable to the geometries of the contact partners. The carbon brushes are initially provided with a flat, circular contact surface. In the case of axial contact, this results in a surface contact with a relatively large contact area between the carbon brush and the end face of the shaft. In the case of radial contact, this results in a line contact with a very small contact area, since the carbon brushes and the shaft only touch in one line.

3.2.3. Effect and Significance of Rotational Speed

Table 5 contains the *p*-values as results of the ANOVA for factor rotational speed on the various features of the electrical impedance. It can be seen that there are no significant effects of factor rotational speed on the features of the impedance.

Table 5. Results of the ANOVA for the factor rotational speed related to different features.

Feature	Symbol	*p*-Value	Significance [4]
Absolute value	$\|Z\|$	0.74181	
Phase	$\varphi(Z)$	0.52112	
Real part	$Re(Z)$	0.18106	
Imaginary part	$Im(Z)$	0.97503	
Resistance	R	0.54324	
Capacitance	C	0.26860	

[4] Significant when p-value < 0.05.

According to the ANOVA, the differences in the main effects as a function of the factor rotational speed shown in Figure 6 do not represent significant effects. Therefore, it can be concluded that the rotational speed of the shaft has no significant effect on the impedance. Nonetheless, it seems generally plausible that rotational-frequency-dependent effects can occur in the impedance data, even if they do not have a significant effect on the impedance in the ANOVA. A suitable analysis for this is a FFT, which as described in Section 3.1, cannot be fully performed within the scope of this work for technical reasons. This could be considered again in future investigations.

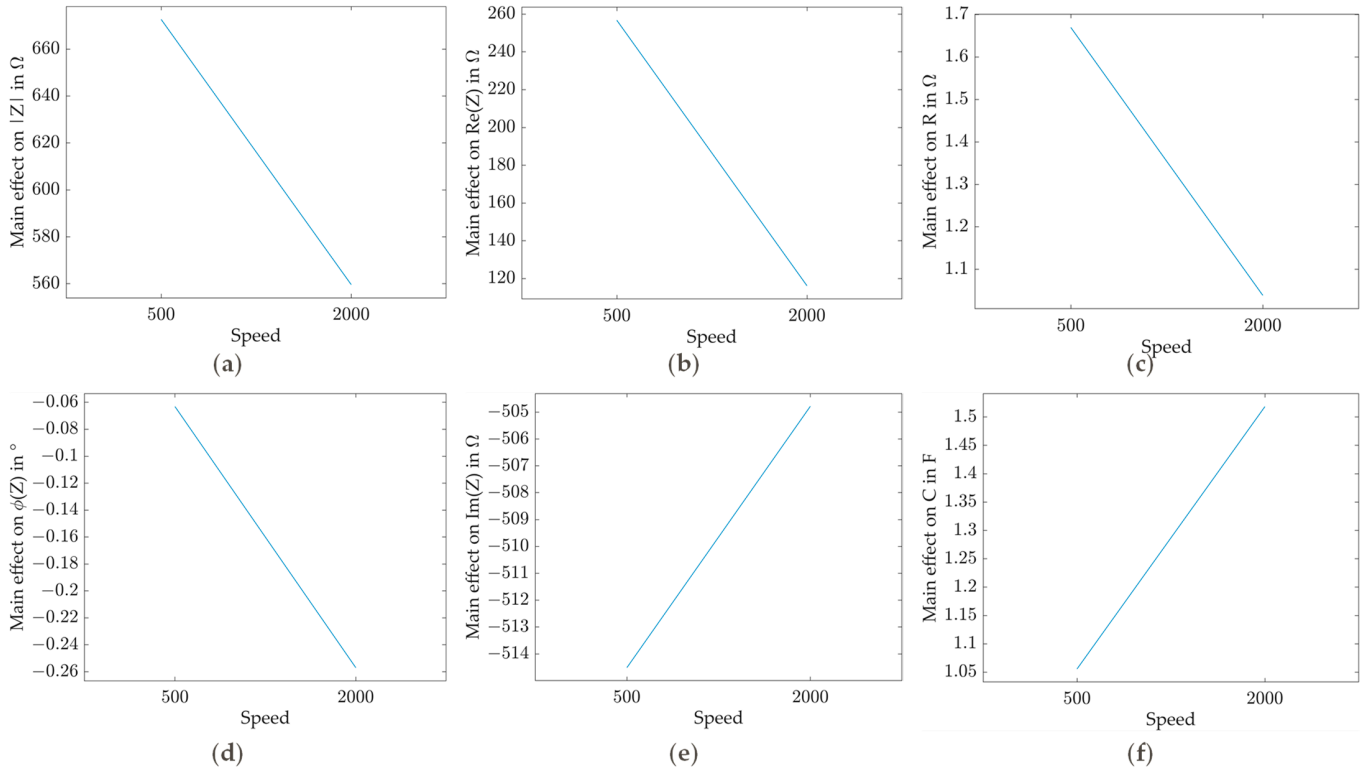

Figure 6. Main effect diagrams of the factor rotational speed for different features: (**a**) No significant effect on $|Z|$; (**b**) No significant effect on $Re(Z)$; (**c**) No significant effect on R; (**d**) No significant effect on $\varphi(Z)$; (**e**) No significant effect on $Im(Z)$; (**f**) No significant effect on C.

3.3. Influence of Runtime and Carrier Frequency on the Electrical Impedance

In the second experimental series, the carrier-frequency-dependent and the runtime-dependent behavior of the impedance is investigated at a constant operating point. The operating point was determined in accordance with the findings obtained in the first experimental series: A silver-graphite carbon brush is operated in axial contact position at 500 rpm, as this represents the most suitable operating condition (see Sections 3.2 and 4). The carrier frequency is swept in a range from 1 kHz to 1 MHz. To investigate the runtime-dependent behavior, the frequency sweeps are repeated at regular intervals over a total period of 120 min.

Figure 7a shows the carrier-frequency-dependent behavior of the absolute value of the impedance for the measurements after different runtimes. A strong frequency dependence can be seen starting between 10 kHz and 100 kHz. From this point on, the magnitude of the impedance increases steeply for all measurements. The measurements after a longer runtime show lower absolute values than measurements after a shorter runtime. Figure 7b shows the carrier-frequency-dependent behavior of the phase of the impedance for the measurements after different runtimes. Here, the results can be divided into two ranges: Up to a frequency between 10 kHz and 100 kHz, the phase angle oscillates strongly around 0°, with outliers up to ± 180°. There is hardly any difference between the measurements at different runtimes. A strong frequency dependence can be seen in the subsequent second range above 100 kHz. Here, the phase angles initially rise and then fall again around 1 MHz. In this range, the measurements after a longer runtime have a larger phase angle than measurements after a shorter runtime. A reliable explanation for the carrier frequency dependence cannot be given conclusively. On one hand, the impedance of the sliding contact can be or is frequency dependent according to the common understanding of impedance. On the other hand, disturbance factors due to—e.g., the cabling or inductances in the system—cannot be excluded. In any case, it is important in the application to check the choice of carrier frequency to avoid unwanted effects and reduce uncertainty.

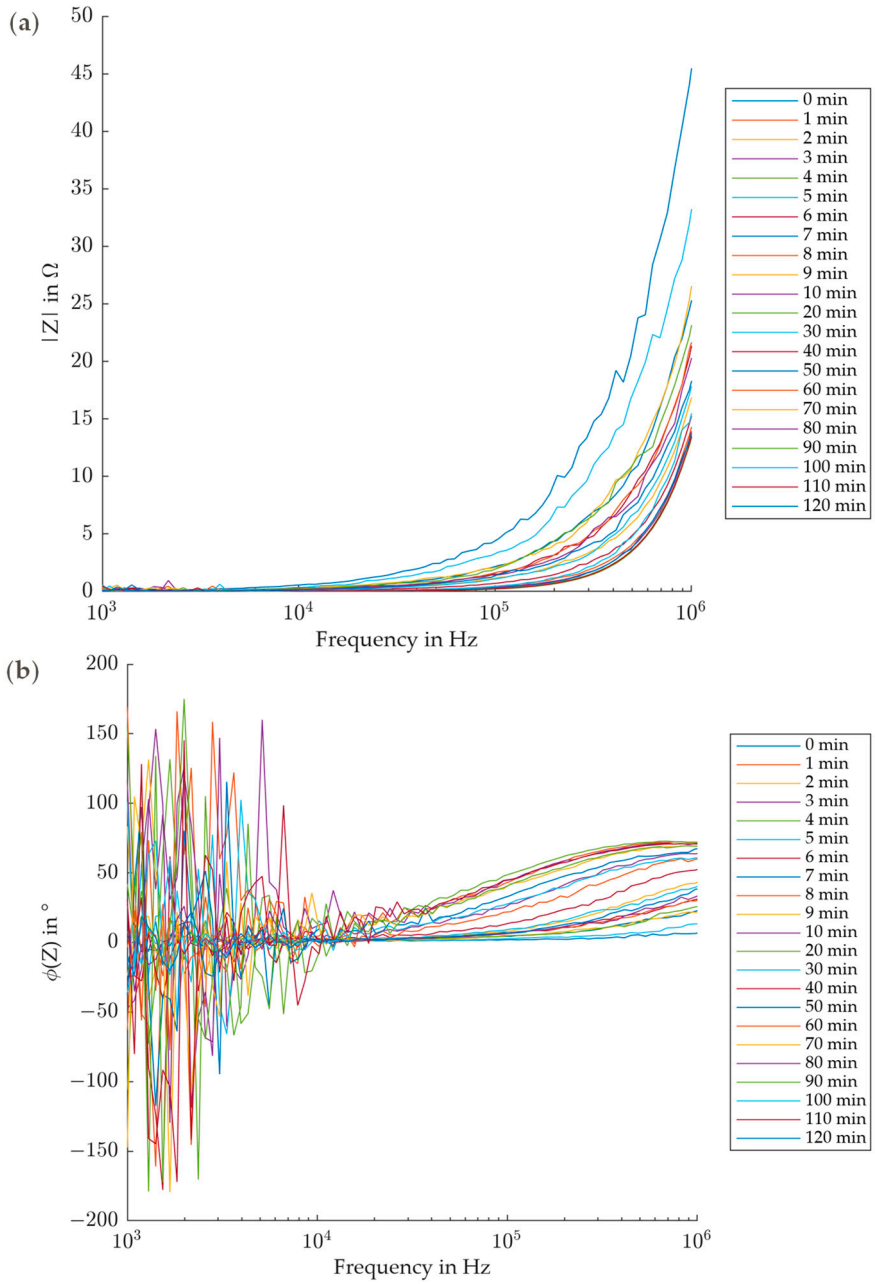

Figure 7. Periodical frequency sweeps (1 kHz to 1 MHz) for a silver graphite carbon brush at 500 rpm in axial contact over a period of 120 min: (**a**) Frequency behavior of $|Z|$; (**b**) Frequency behavior of $\varphi(Z)$.

Compared to the results from the first experimental series (time domain measurement instead of frequency sweeps), it can be seen that the results are matching. The absolute values from Figure 7a at 100 kHz and a short runtime are in the same order of magnitude as the absolute values of the impedance in Figure 3a (approx. 5 Ω). The phase angles from Figure 7b at 100 kHz and a short runtime are in the same order of magnitude as the phase of the impedance in Figure 3a (approx. 0°).

Since it is relatively difficult to compare the effects of different runtimes in Figure 7, further analysis is performed below. An average value of the absolute value of the impedance and an average value of the phase of the impedance are calculated for each frequency sweep measured at a specific runtime. Figure 8a shows the runtime-dependent behavior of the absolute value of the impedance. It can be seen that the absolute value of the impedance decreases with increasing runtime, and approaches a lower boundary. Figure 8b shows

the runtime-dependent behavior of the phase of the impedance. It can be seen that the phase of the impedance increases with increasing runtime, and also appears to potentially approach a boundary. Clear runtime-dependent behavior can be seen for both absolute value and phase of the impedance. This shows that the running-in of new carbon brushes has a measurable influence on the impedance. Carbon brushes of the type used at this specific operating condition start to show a constant impedance behavior after more than 60 min.

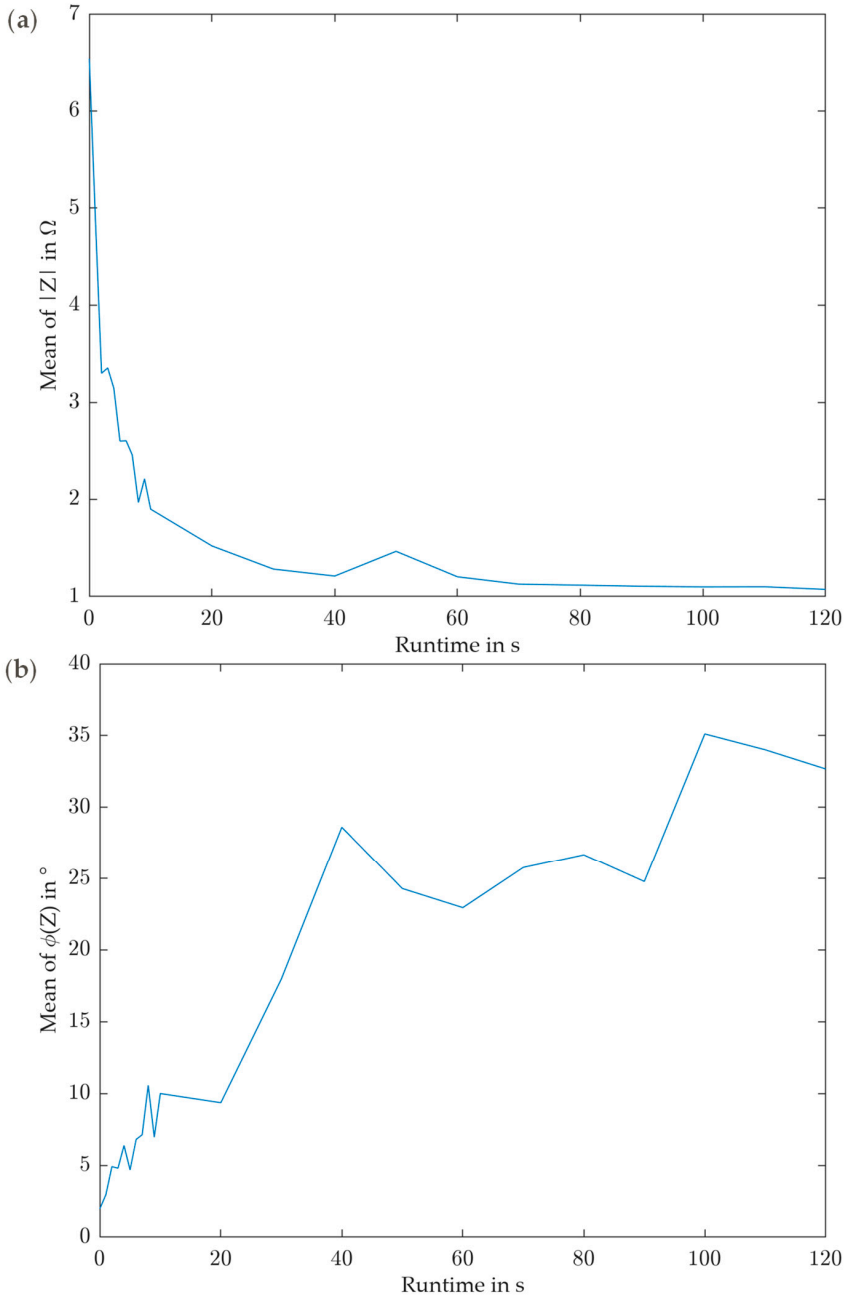

Figure 8. (**a**) Mean of $|Z|$ for the entire frequency sweep (1 kHz to 1 MHz) over a period of 120 min; (**b**) Mean of $\varphi(Z)$ for the entire frequency sweep (1 kHz to 1 MHz) over a period of 120 min.

4. Discussion

From the experimental series carried out, it can be deduced for the impedance behavior of sliding contacts on the basis of a screening design that the material and position of the carbon brush have a significant influence on the impedance. Thus, the impedance of a silver

graphite carbon brush is lower in absolute value and more resistive than a graphite carbon brush. Axial contacting also has a lower, more resistive, and more uniform impedance than radial contacting. In contrast, the rotational speed of the shaft has no significant effect on the impedance. The nature of the effect—e.g., whether it is linear or not—has not been investigated in this screening experiment, and has therefore not been conclusively clarified. For this, a larger number of operating conditions need to be investigated. The carrier frequency used plays a significant role and should always be considered. Furthermore, carbon brushes exhibit measurably verifiable run-in behavior, with the absolute value of the impedance decreasing with runtime, while the phase angle increases with runtime.

For the application as a signal transmission element for the sensory utilization of machine elements, such as rolling element bearings, contacting types with the lowest possible and at the same time uniform impedance are suitable, whereby resistive components are often preferred to capacitive components. This is due to the fact that in the sensory utilization of rolling element bearings, the capacitance represents the quantity of interest; thus, the measurement of the capacitance should be as undistorted as possible. For this reason, carbon brushes made of silver graphite rather than graphite are more suitable for this application. In addition, sliding contacts should—as far as technically possible—be mounted in an axial position; the contact speed plays only a subordinate role. Furthermore, the carrier frequency for the impedance measurement should be carefully selected, and its influence on the impedance behavior of the sliding contact and the rest of the cabling should be considered. Due to the pronounced run-in behavior, relevant impedance measurements should only be performed after the run-in time in order to reduce uncertainty.

Further steps can be derived from this work for further research. Further materials for sliding contacts can be investigated, since only exemplary carbon brushes from an exemplary manufacturer were examined in this research. However, a classification of different materials is not the focus of this work and would go beyond its scope. In addition to the materials for carbon brushes, the materials of the slip ring can also be investigated. In the context of this work, conventional lathed steel was used for the shaft in order to get as close as possible to the materials and machining quality of conventional shafts, and thus reduce the potential integration and transfer effort in a real technical system. However, many parameters exist, such as surface finishes, whose variation would be of interest. Another interesting factor, which was not systematically investigated in this work, is the influence of temperature. In the context of the experiments performed in this work, the surrounding temperature was kept at a constant level. But this can be varied, as can the shaft temperature and thus the contact temperature, and its influence can be analyzed. Two further aspects of investigation relevant to the application are durability tests of carbon brushes and how the impedance behaves over the lifespan, as well as the investigation of the influence of contaminations such as lubricants or other operating fluids. In order to make it as simple as possible to integrate SuME in situ in the process, a solution must also be developed to place sliding contacts as close as possible to the machine element. This includes, placement in the direct proximity of lubricants, and other operating fluids within the technical system, such as a gearbox housing.

Author Contributions: Conceptualization, M.H. and T.S.; methodology, M.H. and T.S.; software, M.H. and T.S.; validation, M.H.; formal analysis, M.H.; investigation, T.S.; resources, M.H. and T.S.; data curation, M.H.; writing—original draft preparation, M.H.; writing—review and editing, M.H., T.S. and E.K.; visualization, M.H.; supervision, E.K.; project administration, M.H.; funding acquisition, E.K. All authors have read and agreed to the published version of the manuscript.

Funding: This research was funded by the Deutsche Forschungsgemeinschaft (DFG, German Research Foundation), grant number 431606807.

Data Availability Statement: The experimental data presented in this study are openly available in TUdatalib at https://doi.org/10.48328/tudatalib-1241 (accessed on 3 October 2023). The software data used in this study are available on request from the corresponding author. The software data are not publicly available due to copyright interests.

Conflicts of Interest: The authors declare no conflict of interest.

Appendix A

Appendix A presents the detailed results of the ANOVA performed in this work. An independent ANOVA is performed for each feature with the help of the 'Statistics and Machine Learning Toolbox' for the software MATLAB R2023a [22]. The resulting p-values are used in Section 3 for the evaluation of the significance of factors. The results of the ANOVA for the feature absolute value of the impedance $|Z|$ is presented in Table A1. The results of the ANOVA for the feature phase angle of the impedance $\varphi(Z)$ is presented in Table A2. The results of the ANOVA for the feature real part of the impedance $Re(Z)$ is presented in Table A3. The results of the ANOVA for the feature imaginary part of the impedance $Im(Z)$ is presented in Table A4. The results of the ANOVA for the feature resistance R is presented in Table A5. The results of the ANOVA for the feature capacitance C is presented in Table A6.

Table A1. Results of the ANOVA for the feature absolute value of the impedance $|Z|$.

	Sum of Squares	DF	Mean Squares	F	p-Value
Material	92,878	1	92,878	0.13629	0.71684
Position	4.9085×10^6	1	4.9085×10^6	7.2027	0.016304
Speed	76,586	1	76,586	0.11238	0.74181
Material and Position	2.4528×10^5	1	2.4528×10^5	0.35992	0.55695
Material and Speed	3.0215×10^6	1	3.0215×10^6	4.4337	0.051384
Position and Speed	9760	1	9760	0.014322	0.90623
Material and Position and Speed	2.4408×10^6	1	2.4408×10^6	3.5816	0.07666
Error	1.0904×10^7	16	6.8149×10^5		
Total	2.1699×10^7	23			

Table A2. Results of the ANOVA for the feature phase angle of the impedance $\varphi(Z)$.

	Sum of Squares	DF	Mean Squares	F	p-Value
Material	1.0989	1	1.0989	8.9809	0.008536
Position	5.0624	1	5.0624	41.372	8.2897×10^{-6}
Speed	0.22537	1	0.22537	1.8418	0.19358
Material and Position	1.2338	1	1.2338	10.083	0.0058736
Material and Speed	0.0051747	1	0.0051747	0.04229	0.83966
Position and Speed	0.6561	1	0.6561	5.3619	0.034181
Material and Position and Speed	0.14021	1	0.14021	1.1458	0.30031
Error	1.9578	16	0.12236		
Total	10.38	23			

Table A3. Results of the ANOVA for the feature real part of the impedance $Re(Z)$.

	Sum of Squares	DF	Mean Squares	F	p-Value
Material	3.3866×10^5	1	3.3866×10^5	5.5927	0.031008
Position	26,062	1	26,062	0.43039	0.52112
Speed	1.1842×10^5	1	1.1842×10^5	1.9557	0.18106
Material and Position	28,688	1	28,688	0.47376	0.50112
Material and Speed	1.7643×10^5	1	1.7643×10^5	2.9136	0.10716
Position and Speed	28,798	1	28,798	0.47558	0.50031
Material and Position and Speed	60,409	1	60,409	0.99762	0.33275
Error	9.6885×10^5	16	60,553		
Total	1.7463×10^6	23			

Table A4. Results of the ANOVA for the feature imaginary part of the impedance $Im(Z)$.

	Sum of Squares	DF	Mean Squares	F	*p*-Value
Material	19,636	1	19,636	0.034968	0.85401
Position	5.1165×10^6	1	5.1165×10^6	9.1115	0.0081578
Speed	567.66	1	567.66	0.0010109	0.97503
Material and Position	1.4106×10^6	1	1.4106×10^6	0.25121	0.62305
Material and Speed	2.3054×10^6	1	2.3054×10^6	4.1055	0.059752
Position and Speed	633.49	1	633.49	0.0011281	0.97362
Material and Position and Speed	2.1593×10^6	1	2.1593×10^6	3.8452	0.067534
Error	8.9846×10^6	16	5.6154×10^5		
Total	1.8728×10^7	23			

Table A5. Results of the ANOVA for the feature resistance R.

	Sum of Squares	DF	Mean Squares	F	*p*-Value
Material	4.5254×10^7	1	4.5254×10^7	0.073189	0.79021
Position	4.2856×10^9	1	4.2856×10^9	6.9311	0.018096
Speed	2.3858×10^8	1	2.3858×10^8	0.38585	0.54324
Material and Position	3.4512×10^7	1	3.4512×10^7	0.055816	0.081623
Material and Speed	2.6144×10^9	1	2.6144×10^9	4.2282	0.05645
Position and Speed	2.3297×10^8	1	2.3297×10^8	0.37678	0.54796
Material and Position and Speed	2.5973×10^9	1	2.5973×10^9	4.2005	0.057175
Error	9.8931×10^9	16	6.1832×10^8		
Total	1.9942×10^{10}	23			

Table A6. Results of the ANOVA for the feature capacitance C.

	Sum of Squares	DF	Mean Squares	F	*p*-Value
Material	3.9386×10^{-11}	1	3.9386×10^{-11}	40.281	9.6967×10^{-6}
Position	3.7262×10^{-11}	1	3.7262×10^{-11}	38.108	1.3379×10^{-5}
Speed	1.2844×10^{-12}	1	1.2844×10^{-12}	1.3136	0.2686
Material and Position	3.7566×10^{-11}	1	3.7566×10^{-11}	38.42	1.2766×10^{-5}
Material and Speed	1.2531×10^{-12}	1	1.2531×10^{-12}	1.2816	0.27429
Position and Speed	1.5714×10^{-12}	1	1.5714×10^{-12}	1.6071	0.22304
Material and Position and Speed	1.6058×10^{-12}	1	1.6058×10^{-12}	1.6422	0.21828
Error	1.5645×10^{-11}	16	9.7778×10^{-13}		
Total	1.3557×10^{-10}	23			

References

1. Anderl, R.; Picard, A.; Wang, Y.; Fleischer, J.; Dosch, S.; Klee, B.; Bauer, J. *Guideline Industrie 4.0: Guiding Principles for the Implementation of Industrie 4.0 in Small and Medium Sized Businesses*; VDMA Verlag GmbH: Frankfurt, Germany, 2016. Available online: https://www.vdma.org/c/document_library/get_file?uuid=71502bd7-5549-7033-5237-549253f1ef0f&groupId=34570 (accessed on 4 October 2023).
2. Hirsch-Kreinsen, H.; Kubach, U.; Stark, R.; von Wichert, G.; Hornung, S.; Hubrecht, L.; Sedlmeir, J.; Steglich, S. *Key Themes of Industry 4.0: Research and Development Needs for Successfull Implementation of Industry 4.0*; Research Council of the Plattform Industrie 4.0: Munich, Germany, 2019. Available online: https://www.plattform-i40.de/IP/Redaktion/EN/Downloads/Publikation/acatech-keythemes-industrie-4-0.pdf?__blob=publicationFile&v=1 (accessed on 4 October 2023).
3. Fleischer, J.; Klee, B.; Spohrer, A.; Merz, S. Guideline Sensors for Industrie 4.0: Options for Cost-Efficient Sensor Systems. 2018. Available online: https://vdma.org/viewer/-/v2article/render/1132021 (accessed on 16 February 2022).
4. Stücheli, M.; Meboldt, M. Mechatronic Machine Elements: On Their Relevance in Cyber-Physical Systems. In *Smart Product Engineering, Proceedings of the 23rd CIRP Design Conference, CIRP Design Conference, Bochum, Germany, 11–13 March 2013*; Abramovici, M., Stark, R., Eds.; Springer: Berlin/Heidelberg, Germany, 2013; pp. 263–272, ISBN 978-3-642-30816-1.
5. Vorwerk-Handing, G.; Gwosch, T.; Schork, S.; Kirchner, E.; Matthiesen, S. Classification and examples of next generation machine elements. *Forsch. Im Ingenieurwesen* **2020**, *84*, 21–32. [CrossRef]
6. Furtmann, A.; Poll, G. Evaluation of Oil-Film Thickness Along the Path of Contact in a Gear Mesh by Capacitance Measurement. *Tribol. Online* **2016**, *11*, 189–194. [CrossRef]

7. Hausmann, M.; Kirchner, E. Investigation of the electrical impedance of the gear mesh of helical gears in an industrial gearbox. In Proceedings of the International Conference on Gears 2023, Garching/Munich, Germany, 13–15 September 2023; VDI Wissensforum GmbH, Ed.; VDI Verlag GmbH: Düsseldorf, Germany, 2023; pp. 1173–1179, ISBN 978-3-18-092422-9.
8. Werner, M.; Graf, S.; Oehler, M.; Koch, O. Investigation of the electrical behavior of a spur gear stage pair by means of im-pedance measurements. In Proceedings of the International Conference on Gears 2023, Garching/Munich, Germany, 13–15 September 2023; VDI Wissensforum GmbH, Ed.; VDI Verlag GmbH: Düsseldorf, Germany, 2023; pp. 67–80, ISBN 978-3-18-092422-9.
9. Lane, T.B.; Hughes, J.R. A study of the oil-film formation in gears by electrical resistance measurements. *Br. J. Appl. Phys.* **1952**, *3*, 315–318. [CrossRef]
10. MacConochie, I.O.; Cameron, A. The Measurement of Oil-Film Thickness in Gear Teeth. *J. Basic Eng.* **1960**, *82*, 29–34. [CrossRef]
11. Machado, C.; Guessasma, M.; Bellenger, E.; Bourbatache, K.; Bourny, V.; Fortin, J. Diagnosis of faults in the bearings by electrical measures and numerical simulations. *Mech. Ind.* **2014**, *15*, 383–391. [CrossRef]
12. Maruyama, T.; Maeda, M.; Nakano, K. Lubrication Condition Monitoring of Practical Ball Bearings by Electrical Impedance Method. *Tribol. Online* **2019**, *14*, 327–338. [CrossRef]
13. Martin, G.; Becker, F.M.; Kirchner, E. A novel method for diagnosing rolling bearing surface damage by electric impedance analysis. *Tribol. Int.* **2022**, *170*, 107503. [CrossRef]
14. Maruyama, T.; Radzi, F.; Sato, T.; Iwase, S.; Maeda, M.; Nakano, K. Lubrication Condition Monitoring in EHD Line Contacts of Thrust Needle Roller Bearing Using the Electrical Impedance Method. *Lubricants* **2023**, *11*, 223. [CrossRef]
15. De Gaetano, D.; Zhu, W.; Sun, X.; Chen, X.; Griffo, A.; Jewell, G.W. Experimental Ball Bearing Impedance Analysis Under Different Speed and Electrical Conditions. *IEEE Trans. Dielect. Electr. Insul.* **2023**, *30*, 1312–1321. [CrossRef]
16. HCP Sense GmbH. Products: HCP Sense Technology Works with any Rolling Bearing. Available online: https://hcp-sense.com/en/products/ (accessed on 28 September 2023).
17. Holm, R. *Electric Contacts: Theory and Application*; Springer: Berlin/Heidelberg, Germany, 1967; ISBN 978-3-642-05708-3.
18. Vinaricky, E.; Faber, M. Gleitender Kontakt: Kohlebürsten und Schleifstücke. In *Elektrische Kontakte, Werkstoffe und Anwen-Dungen: Grundlagen, Technologien, Prüfverfahren, 3. Auflage*; Vinaricky, E., Ed.; Springer Vieweg: Berlin/Heidelberg, Germany, 2016; pp. 191–222, ISBN 978-3-642-45427-1.
19. Chevallier, E.; Garcia, T.; Mohamed, S.A. Electromechanical Study of a Ring-Brush Sliding Contact. *arXiv* **2023**. [CrossRef]
20. Chevallier, E. Mechanical Model of the Electrical Response from a Ring–Wire Sliding Contact. *Tribol. Trans.* **2020**, *63*, 215–221. [CrossRef]
21. Dean, A.; Voss, D.; Draguljić, D. *Design and Analysis of Experiments*; Springer International Publishing: Cham, Switzerland, 2017; ISBN 978-3-319-52248-7.
22. MathWorks Inc. Anova: Analysis of Variance for Linear Regression Model. Available online: https://de.mathworks.com/help/stats/linearmodel.anova.html (accessed on 25 October 2023).
23. Josef Mack GmbH & Co., KG. Carbon Brushes. Available online: https://www.mackgermany.com/assets/files/downloads/Mack_Kohleb%C3%BCrsten_ENGL_web2.pdf (accessed on 28 September 2023).
24. Kummer, J. Random Number Generator. Available online: https://rechneronline.de/random-numbers/ (accessed on 11 August 2022).
25. 25. Zurich Instruments AG. MFIA: 500 kHz/5 MHz Impedance Analyzer. Available online: https://www.zhinst.com/europe/en/products/mfia-impedance-analyzer (accessed on 28 September 2023).
26. Klotz, D. Impedance Measurements on Grounded Components. Available online: https://www.zhinst.com/europe/en/blogs/impedance-measurements-grounded-components (accessed on 28 September 2023).